

Measurement of the Proton and Deuteron Spin Structure Function g_1 in the Resonance Region

K. Abe,¹⁵ T. Akagi,^{12,15} P. L. Anthony,¹² R. Antonov,¹¹ R. G. Arnold,¹ T. Averett,^{16,‡‡} H. R. Band,¹⁸ J. M. Bauer,⁷ H. Borel,⁵ P. E. Bosted,¹ V. Breton,³ J. Button-Shafer,⁷ J. P. Chen,^{16,8} T. E. Chupp,⁸ J. Clendenin,¹² C. Comptour,³ K. P. Coulter,⁸ G. Court,^{12,*} D. Crabb,¹⁶ M. Daoudi,¹² D. Day,¹⁶ F. S. Dietrich,⁶ J. Dunne,¹ H. Dutz,^{12,**} R. Erbacher,^{12,13} J. Fellbaum,¹ A. Feltham,² H. Fonvieille,³ E. Frlsz,¹⁶ D. Garvey,⁹ R. Gearhart,¹² J. Gomez,⁴ P. Grenier,⁵ K. A. Griffioen,^{11,17} S. Hoibraten,^{16,§} E. W. Hughes,^{12,‡‡} C. E. Hyde-Wright,¹⁰ J. R. Johnson,¹⁸ D. Kawall,¹³ A. Klein,¹⁰ S. E. Kuhn,¹⁰ M. Kuriki,¹⁵ R. Lindgren,¹⁶ T. J. Liu,¹⁶ R. M. Lombard-Nelsen,⁵ J. Marroncle,⁵ T. Maruyama,¹² X. K. Maruyama,⁹ J. McCarthy,¹⁶ W. Meyer,^{12,**} Z.-E. Meziani,^{13,14} R. Minehart,¹⁶ J. Mitchell,⁴ J. Morgenstern,⁵ G. G. Petratos,^{12,‡} R. Pitthan,¹² D. Pocanic,¹⁶ C. Prescott,¹² R. Prepost,¹⁸ P. Raines,¹¹ B. A. Raue,^{10,†} D. Reyna,¹ A. Rijllart,^{12,††} Y. Roblin,³ L. S. Rochester,¹² S. E. Rock,¹ O. A. Rondon,¹⁶ I. Sick,² L. C. Smith,¹⁶ T. B. Smith,⁸ M. Spengos,^{1,11} F. Staley,⁵ P. Steiner,² S. St.Lorant,¹² L. M. Stuart,¹² F. Suekane,¹⁵ Z. M. Szalata,¹ H. Tang,¹² Y. Terrien,⁵ T. Usher,¹² D. Walz,¹² F. Wesselmann,¹⁰ J. L. White,^{1,12} K. Witte,¹² C. C. Young,¹² B. Youngman,¹² H. Yuta,¹⁵ G. Zapalac,¹⁸ B. Zihlmann,² D. Zimmermann¹⁶
(E143 Collaboration)

¹The American University, Washington, D.C. 20016

²Institut für Physik der Universität Basel, CH-4056 Basel, Switzerland

³LPC IN2P3/CNRS, University Blaise Pascal, F-63170 Aubiere Cedex, France

⁴TJNAF, Newport News, Virginia 23606

⁵DAPNIA-Service de Physique Nucleaire Centre d'Etudes de Saclay, F-91191 Gif/Yvette, France

⁶Lawrence Livermore National Laboratory, Livermore, California 94550

⁷University of Massachusetts, Amherst, Massachusetts 01003

⁸University of Michigan, Ann Arbor, Michigan 48109

⁹Naval Postgraduate School, Monterey, California 93943

¹⁰Old Dominion University, Norfolk, Virginia 23529

¹¹University of Pennsylvania, Philadelphia, Pennsylvania 19104

¹²Stanford Linear Accelerator Center, Stanford, California 94309

¹³Stanford University, Stanford, California 94305

¹⁴Temple University, Philadelphia, Pennsylvania 19122

¹⁵Tohoku University, Sendai 980, Japan

¹⁶University of Virginia, Charlottesville, Virginia 22901

¹⁷The College of William and Mary, Williamsburg, Virginia 23187

¹⁸University of Wisconsin, Madison, Wisconsin 53706

(Accepted in Phys. Rev. Lett.)

We have measured the proton and deuteron spin structure functions g_1^p and g_1^d in the region of the nucleon resonances for $W^2 < 5 \text{ GeV}^2$ and $Q^2 \simeq 0.5$ and $Q^2 \simeq 1.2 \text{ GeV}^2$ by inelastically scattering 9.7 GeV polarized electrons off polarized $^{15}\text{NH}_3$ and $^{15}\text{ND}_3$ targets. We observe significant structure in g_1^p in the resonance region. We have used the present results, together with the deep-inelastic data at higher W^2 , to extract $\Gamma(Q^2) \equiv \int_0^1 g_1(x, Q^2) dx$. This is the first information on the low- Q^2 evolution of Γ toward the Gerasimov-Drell-Hearn limit at $Q^2 = 0$.

The nucleon spin structure functions g_1 and g_2 have been and continue to be intensively studied via deep-inelastic lepton scattering [1–6]; however, they remain largely undetermined in the resonance region, where the squared invariant mass of the final state W^2 is less than 4 GeV². Here, g_1 and g_2 can be used to investigate the helicity structure of the resonance transition amplitudes. States of definite spin and parity are more easily understood in terms of the virtual photon asymmetries [7]

$$\begin{aligned} A_1(x, Q^2) &= \frac{\sigma_{1/2} - \sigma_{3/2}}{\sigma_{1/2} + \sigma_{3/2}} = \frac{1}{F_1} \left[g_1 - \frac{Q^2}{\nu^2} g_2 \right] \quad \text{and} \\ A_2(x, Q^2) &= \frac{\sigma_{LT}}{\sigma_T} = \frac{\sqrt{Q^2}}{\nu F_1} [g_1 + g_2], \end{aligned} \quad (1)$$

in which Q^2 is the squared four-momentum transfer, ν is the energy transfer, $x = Q^2/2M\nu$, M is the nucleon mass, and the structure functions F_1 , g_1 and g_2 depend on both x (or W^2) and Q^2 . The cross sections $\sigma_{1/2}$ and $\sigma_{3/2}$ measure the strength of virtual transverse photon absorption leading to final-state spin projections of $\frac{1}{2}$ and $\frac{3}{2}$. The cross sections σ_L , $\sigma_T \equiv (\sigma_{1/2} + \sigma_{3/2})/2$, and σ_{LT} measure longitudinal, transverse and interference photon absorptions. Positivity limits require that $|A_1| \leq 1$ and $|A_2| \leq \sqrt{R(x, Q^2)}$, in which $R \equiv \sigma_L/\sigma_T$. The excitation of the $\Delta(1232)$ resonance (spin- $\frac{3}{2}$) allows for both $\frac{1}{2}$ and $\frac{3}{2}$ spin projections, and at low Q^2 is expected to be primarily a magnetic dipole transition, for which $\sigma_{3/2}/\sigma_{1/2} = 3$ and $A_1 = -\frac{1}{2}$. On the other hand, the $S_{11}(1535)$ resonance has no spin- $\frac{3}{2}$ projection, so A_1 should be unity. The observed values of A_1 in the resonance region are a combination of asymmetries for individual resonances and for the nonresonant background. The goals of the present measurements are to gain a better understanding of the resonances and to determine their influence on the deep-inelastic results, both in terms of radiative corrections and the evolution of $\Gamma(Q^2) \equiv \int_0^1 g_1(x, Q^2) dx$. Although the resonant contribution to Γ is insignificant at high Q^2 , it dominates the integral below about $Q^2 = 0.5$ GeV². In fact, the limits set by the Gerasimov-Drell-Hearn (GDH) sum rule [8] indicate that $\Gamma(Q^2)$ should change sign in the region $0 < Q^2 < 1$ GeV² and approach zero as $Q^2 \rightarrow 0$.

The data for the present analysis are part of the E143 data set [5,6] taken with a 9.7 GeV polarized electron beam (average polarization 85%) and cryogenic ¹⁵NH₃ and ¹⁵ND₃ targets (average polarizations of 65% and 25%, respectively). The data taken with the two spectrometers at 4.5° and 7° corresponded to $Q^2 \simeq 0.5$ and 1.2 GeV² in the resonance region.

Since these data were taken with longitudinal target polarization only, the determination of g_1 or A_1 requires additional assumptions about either g_2 or A_2 . We extract g_1 rather than A_1 because g_1 is significantly less affected by our lack of knowledge of g_2 or A_2 . We set $A_2 = 0$ (corresponding to $g_1 = -g_2$) in our analy-

sis. This is motivated by the fact that $|A_2| \leq \sqrt{R}$ and existing data [9] indicate that R is small in the resonance region ($R = 0.06 \pm 0.02$ for $1 < Q^2 < 8$ GeV² and $W^2 < 3$ GeV²). We have explored the sensitivity to A_2 by considering the alternate possibilities $g_2 = 0$ and $g_2 = g_2^{\text{WW}} = -g_1 + \int_x^1 g_1(x')/x' dx'$, the Wandzura-Wilczek [10] twist-two form. Maximum deviations in g_1 from the $A_2 = 0$ case define the systematic errors due to uncertainty in A_2 . Even if A_2 were as large as 0.3, the extracted values of g_1 would shift by less than 0.014, which is small compared to the statistical errors on each point.

We have extracted g_1 from the absolute cross section differences for electron and nucleon spins aligned along the beam axis either parallel ($\uparrow\uparrow$) or antiparallel ($\uparrow\downarrow$) to each other [7]:

$$\begin{aligned} \frac{1}{\sigma_M} \frac{d\sigma^{\uparrow\downarrow(\uparrow\uparrow)}}{d\Omega dE'} &= \frac{F_2}{\nu} + \frac{2}{M} \tan^2\left(\frac{\theta}{2}\right) F_1 + (-) \frac{2}{M\nu} \tan^2\left(\frac{\theta}{2}\right) \\ &\times \left[(E + E' \cos\theta + Q^2/\nu) g_1 - \sqrt{Q^2} F_1 A_2 \right] \end{aligned} \quad (2)$$

in which σ_M is the Mott scattering cross section, E (E') is the initial (final) electron energy, θ is the laboratory scattering angle, $\nu = E - E'$, and F_1 and F_2 are the unpolarized structure functions.

This method requires good knowledge of spectrometer acceptances, the number density of polarizable protons or deuterons in the target, and detector efficiencies. Alternatively, one could extract g_1 from the count rate asymmetry as in Ref. [5,6]; however, the dilution factor (the fraction of scatterings coming from a polarizable nucleon in the target) is needed in this case, which is more difficult to obtain reliably in the resonance region. Nevertheless, when we tried both methods, we found that they agreed to within a fraction of the statistical errors on each point (typically better than 3%).

As the first step to determine the absolute cross section differences, we calculated the raw count differences per incident charge $N^{\uparrow\downarrow}/q^{\uparrow\downarrow} - N^{\uparrow\uparrow}/q^{\uparrow\uparrow}$, with each term corrected for dead-time in the trigger electronics. For each electron, W^2 was calculated using the momentum and scattering angle determined from tracking. The data were binned in W^2 , normalized by the product of target and beam polarizations and corrected for absolute spectrometer efficiency. Each detector's efficiency was determined by making a strict cut to select good electron events without using one of the detectors and checking how often that detector registered the electron. The absolute spectrometer efficiency is the product of all of the individual detector efficiencies (no evidence for correlations between them was found) [11].

Fully corrected cross section differences $d\Delta\sigma/dE'd\Omega$ were obtained with the help of a Monte Carlo simulation. This simulation was used to normalize the raw data for target density and spectrometer acceptance. The normalized data were then corrected for radiative and resolution effects by an additive term determined from the

Monte Carlo routine. Small corrections for polarized ^{15}N and ^{14}N in the target (and ^1H in the case of the deuteron) were applied as in Ref. [5].

The Monte Carlo code simulated all relevant aspects of the experiment and was able to predict total count rates and count rate differences based on a set of input tables of cross sections and asymmetries. The unpolarized cross sections were calculated from a fit by Stuart *et al.* [12]. The asymmetry tables were calculated from a combination of resonant and non-resonant contributions. The non-resonant part came from a parameterization of all existing deep inelastic data (Fit III of Ref. [6]), which was extrapolated into the resonance region. The asymmetry of the $\Delta(1232)$ resonance was fixed at $A_1 = -0.5$. The contribution to the asymmetry from all other resonances was approximated by two constant values (one for the region below $W^2 = 2.6 \text{ GeV}^2$ and the other for the region above $W^2 = 3.2 \text{ GeV}^2$) and a linear interpolation between them. This simple parameterization was sufficient to achieve a reasonable fit to the data for the purpose of radiative and smearing corrections. The quality of the Monte Carlo results was also tested by comparing the predicted and measured total count rates and (quasi-) elastic asymmetries. We found good agreement within the statistical uncertainty of the data.

The full model was used to calculate cross sections and asymmetries both in lowest order of QED (Born approximation) and with full radiative corrections following the prescription by Shumeiko *et al.* [13]. We used the peaking approximation after convincing ourselves that the full code produced negligible differences. The radiated cross sections and asymmetries were tabulated as input for the Monte Carlo code, while the Born cross sections and asymmetries were compared with the Monte Carlo output to determine the normalization factor and the additive correction for the raw data.

Fig. 1 shows g_1 obtained from cross section differences for proton and deuteron (per nucleon) measured with the two spectrometers as a function of W^2 . The full length of the error bars corresponds to the statistical and systematic uncertainties added in quadrature. The cross bars indicate statistical errors alone, which dominate the total errors. Plotted as triangles are the data of Baum *et al.* [14] taken at similar kinematics and converted to g_1 for comparison by assuming $A_2 = 0$. Within errors, the two measurements agree well. The solid lines show the Monte Carlo simulation. The dashed curve is a calculation using the code AO by Burkert and Li [15]. This calculation does not adequately describe the data above $W^2 = 3 \text{ GeV}^2$, because the non-resonant background contains only the single π Born term. Although AO describes the resonance region at higher Q^2 rather well, there is a significant discrepancy in the second resonance region ($2 < W^2 < 3 \text{ GeV}^2$) at the lower Q^2 .

Extracting the total (resonant plus non-resonant) A_1

at fixed W^2 from the relationship $g_1 = \frac{\nu^2}{\nu^2 + Q^2}(A_1 + \frac{Q}{\nu}A_2)F_1$ requires several simplifying assumptions. We assume $A_2 = 0$, $R = 0.25/Q^2$ for the non-resonant cross section [12], and $R = 0$ for the resonant cross section [9] and obtain F_1 from measured values of F_2 and R . In that case, all data for both proton and deuteron are consistent with $A_1^\Delta = -\frac{1}{2}$ with a relative uncertainty of 40-100%. This is also the asymmetry that AO predicts. On the other hand, A_1 in the region $W^2 = 2 - 3 \text{ GeV}^2$, which is dominated by the S_{11} and D_{13} resonances, is surprisingly high. Here the proton data at 4.5° and 7° are consistent with $A_1 = 0.9 \pm 0.2$, which is close to the positivity limit and well above the AO prediction. This could indicate a significant contribution from A_2 , from a non-resonant asymmetry that is much larger than expected from deep-inelastic extrapolations, or from a stronger than expected contribution from S_{11} for which $A_1 = 1$. The smaller corresponding asymmetry for the deuteron ($A_1 = 0.3 \pm 0.2$) may arise from Fermi smearing or a genuine n-p difference. More detailed information on the asymmetries of individual resonances and the non-resonant background are expected once high-precision, semi-exclusive data from TJNAF become available.

Fig. 2 shows the integrals $\Gamma(Q^2)$ for proton and neutron, evaluated at the average Q^2 for the resonance region ($M^2 < W^2 < 4 \text{ GeV}^2$). We summed our resonance results directly (where Q^2 does not vary much) and then added a contribution from smaller x (larger W^2) at the same fixed Q^2 taken from Fit III to the world's deep-inelastic g_1 data [6]. The neutron integrals were derived assuming a 5% D-state probability for the deuteron. The statistical errors assigned to Fit III [6] at given values of x and Q^2 corresponded to the kinematically closest E143 data points at 9.7 or 16 GeV, which dominated the fit in this region. Systematic errors were calculated using the systematic uncertainties for the measured g_1 in the resonance region added linearly to the systematic errors for the deep-inelastic region, which are highly correlated with each other. Extrapolation errors for the region below the last measured datum at $x = 0.03$ were taken to be as large as the value that Fit III yields for $x < 0.03$.

Although several models for the Q^2 evolution of $\Gamma(Q^2)$ exist [16–20], we show here only two representative ones, together with the evolution [21] of the world's deep-inelastic data due to the changing coupling constant α_S . Although the GDH sum rule is strictly valid only at $Q^2 = 0$ where $\Gamma(Q^2)$ vanishes, it can be used to predict the slope of $\Gamma(Q^2)$ for small Q^2 . The solid line at low Q^2 in Fig. 2 shows $\Gamma = -\kappa^2 Q^2 / 8M^2$ in which κ is the anomalous magnetic moment of either the proton or neutron. Burkert and Ioffe [19] consider the contributions from the resonances using the code AO, and the nonresonant contributions using a simple higher-twist-type form fitted to the deep-inelastic data. Their model is constrained to fit both the GDH and the deep-inelastic limits, and it

describes the data quite well. Soffer and Teryaev [20] assume that the integral over $g_1 + g_2$ varies smoothly from high Q^2 where $g_2 \approx 0$ down to $Q^2 = 0$. Using their simple prediction for this integral and subtracting the contribution from g_2 alone using the Burkhardt-Cottingham sum rule [22], gives the dashed curve in Fig. 2b, which also agrees quite well with our data.

The present spin structure function data in the region of the nucleon resonances allow us to determine the integrals $\Gamma(Q^2)$ for the first time at Q^2 below 2 GeV². In contrast to the nearly flat behavior in the deep-inelastic region above $Q^2 = 2$ GeV², Γ varies rapidly below $Q^2 = 2$ GeV². Models that interpolate between the deep-inelastic and GDH limits describe the data quite well in this non-perturbative regime.

This work was supported by the Department of Energy; the National Science Foundation; the Schweizerische Nationalfonds; the Commonwealth of Virginia; the Centre National de la Recherche Scientifique and the Commissariat a l'Energie Atomique (French groups); the Japanese Ministry of Education, Science, and Culture; and the Jeffress Memorial Trust (W&M).

* Permanent address: Oliver Lodge Lab, University of Liverpool, Liverpool, U. K.

** Permanent address: University of Bonn, D-53113 Bonn, Germany.

§ Permanent address: FFIYM, P.O. Box 25, N-2007 Kjeller, Norway.

‡ Present address: Kent State University, Kent, Ohio 44242.

†† Permanent address: CERN, 1211 Geneva 23, Switzerland.

† Permanent address: Florida International University, Miami, FL 33199.

‡‡ Present Address: California Institute of Technology, Pasadena, CA 91125

- [1] E80, M.J. Alguard, *et al.*, Phys. Rev. Lett. **37**, 1261 (1976); Phys. Rev. Lett. **41**, 70 (1978); E130, G. Baum, *et al.*, Phys. Rev. Lett. **51**, 1135 (1983);
 [2] EMC, J. Ashman *et al.*, Phys. Lett. **B206**, 364 (1988); Nucl. Phys. **B328**, 1 (1989).
 [3] E142, P. L. Anthony *et al.*, Phys. Rev. Lett. **71**, 959 (1993).
 [4] SMC, B. Adeva *et al.*, Phys. Lett. **B302**, 533 (1993); D. Adams *et al.*, Phys. Lett. **B329**, 399 (1994); **B336**, 125 (1994); **B357**, 248 (1995).
 [5] E143, K. Abe *et al.*, Phys. Rev. Lett. **74**, 346 (1995); Phys. Rev. Lett. **75**, 25 (1995); Phys. Rev. Lett. **76**, 587 (1996).
 [6] E143, K. Abe *et al.*, Phys. Lett. **B364**, 61 (1995).
 [7] R. D. Roberts, The Structure of the Proton, Cambridge Univ. Press (1990).

- [8] S. Gerasimov, Sov. J. Nucl. Phys. **2**, 430 (1966); S.D. Drell and A.C. Hearn, Phys. Rev. Lett. **16**, 908 (1966).
 [9] C. Keppel, PhD Thesis, American University, 1994; unpublished.
 [10] S. Wandzura and F. Wilczek, Phys. Lett. **B72**, 195 (1977).
 [11] P. Raines, PhD Thesis, University of Pennsylvania, 1996; unpublished.
 [12] L.M. Stuart, *et al.*, SLAC-PUB-7391 (1996), hep-ph 9612416; submitted to Phys. Rev. D.
 [13] T. V. Kukhto and N. M. Shumeiko, Nucl. Phys. **B219**, 412 (1983); I. V. Akusevich and N. M. Shumeiko, J. Phys. **G20**, 513 (1994).
 [14] G. Baum *et al.*, Phys. Rev. Lett. **45**, 2000 (1980).
 [15] V. Burkert and Z.-J. Li, Phys. Rev. D **47**, 46 (1993).
 [16] V. Bernard, N. Kaiser and U.-G. Meissner, Phys. Rev. D **48**, 3062 (1993).
 [17] X. Ji and P. Unrau, Phys. Lett. **B333**, 228 (1994).
 [18] Z.-P. Li and Zh. Li, Phys. Rev. D **50**, 3119 (1994).
 [19] V.D. Burkert and B.L. Ioffe, Phys. Lett. **B296** 223, (1992); CEBAF Preprint PR-93-034.
 [20] J. Soffer and O.V. Teryaev, Phys. Rev. D **51**, 25 (1995).
 [21] S.A. Larin, Phys. Lett. **B334**, 192 (1994).
 [22] H. Burkhardt and W. N. Cottingham, Ann. Phys. **56**, 453 (1970).

TABLE I. Integrals $\Gamma(Q^2)$ of the structure functions g_1 for the proton (p), deuteron (d) and neutron (n). The measured sum Γ_{res} for the resonance region ($W^2 < 4$ GeV²) is listed separately from the totals Γ_{tot} , which includes the deep-inelastic region as given by fits to the world's data.

Q^2 (GeV ²)		$\Gamma_{res} (\pm\text{stat.}\pm\text{syst.})$	$\Gamma_{tot} (\pm\text{stat.}\pm\text{syst.})$
0.5	p	0.026±0.008±0.008	0.049 ± 0.008 ± 0.013
0.5	d	0.000±0.013±0.008	0.003 ± 0.013 ± 0.010
0.5	n	-0.026±0.028±0.020	-0.043 ± 0.029 ± 0.025
1.2	p	0.040±0.003±0.004	0.100 ± 0.005 ± 0.012
1.2	d	0.026±0.006±0.004	0.043 ± 0.008 ± 0.007
1.2	n	0.016±0.013±0.010	-0.006 ± 0.019 ± 0.020

TABLE II. Fully corrected cross section differences $d(\sigma^{\uparrow\downarrow} - \sigma^{\uparrow\uparrow})/dE'd\Omega \equiv \Delta\sigma$ (nb/GeV-sr) and structure functions g_1 for the proton in the resonance region. Listed are the data for the 4.5° and 7.0° spectrometers. The values of Q^2 and W^2 (GeV 2) are given at bin centers. The additive correction $\Delta\sigma_R$ includes both radiative effects and resolution corrections.

	W^2	Q^2	$\Delta\sigma$	$\Delta\sigma_R$	g_1
4.5°	1.31	0.55	-74 ± 133	-714	$-0.013\pm 0.023\pm 0.023$
	1.69	0.54	-289 ± 116	-244	$-0.070\pm 0.028\pm 0.006$
	2.06	0.53	627 ± 106	282	$0.197\pm 0.033\pm 0.039$
	2.44	0.52	828 ± 109	229	$0.320\pm 0.042\pm 0.046$
	2.81	0.50	245 ± 108	-120	$0.113\pm 0.050\pm 0.025$
	3.19	0.49	120 ± 80	-166	$0.064\pm 0.043\pm 0.034$
	3.56	0.48	75 ± 78	-59	$0.046\pm 0.048\pm 0.015$
	3.94	0.47	-2 ± 79	-29	$-0.001\pm 0.055\pm 0.010$
	4.31	0.46	158 ± 68	-7	$0.123\pm 0.053\pm 0.015$
	4.69	0.45	124 ± 66	-10	$0.106\pm 0.057\pm 0.010$
7°	1.19	1.28	-4 ± 5	-19	$-0.003\pm 0.003\pm 0.003$
	1.56	1.26	-8 ± 16	-49	$-0.007\pm 0.014\pm 0.005$
	1.94	1.23	43 ± 12	4	$0.043\pm 0.012\pm 0.015$
	2.31	1.20	162 ± 16	45	$0.193\pm 0.020\pm 0.031$
	2.69	1.18	121 ± 16	3	$0.165\pm 0.022\pm 0.016$
	3.06	1.15	95 ± 15	-12	$0.147\pm 0.024\pm 0.019$
	3.44	1.12	57 ± 15	1	$0.098\pm 0.026\pm 0.009$
	3.81	1.09	70 ± 15	2	$0.134\pm 0.029\pm 0.012$
	4.19	1.07	110 ± 15	5	$0.233\pm 0.031\pm 0.025$
	4.56	1.04	83 ± 14	4	$0.193\pm 0.033\pm 0.020$
4.94	1.01	63 ± 14	3	$0.158\pm 0.036\pm 0.022$	

TABLE III. Same as Table 2, but for the deuteron.

	W^2	Q^2	$\Delta\sigma$	$\Delta\sigma_R$	g_1
4.5°	1.31	0.55	-195 ± 207	-397	$-0.034\pm 0.036\pm 0.021$
	1.69	0.54	-190 ± 185	-211	$-0.046\pm 0.045\pm 0.015$
	2.06	0.53	401 ± 163	80	$0.126\pm 0.051\pm 0.016$
	2.44	0.52	127 ± 165	43	$0.049\pm 0.064\pm 0.007$
	2.81	0.50	-41 ± 145	-34	$-0.019\pm 0.067\pm 0.005$
	3.19	0.49	166 ± 128	-32	$0.089\pm 0.069\pm 0.013$
	3.56	0.48	36 ± 120	-17	$0.022\pm 0.074\pm 0.004$
	3.94	0.47	-8 ± 112	-14	$-0.006\pm 0.078\pm 0.002$
	4.31	0.46	-27 ± 101	-9	$-0.021\pm 0.078\pm 0.003$
	4.69	0.45	67 ± 97	-9	$0.058\pm 0.084\pm 0.007$
7°	1.19	1.28	79 ± 24	18	$0.053\pm 0.016\pm 0.010$
	1.56	1.26	1 ± 21	-30	$0.001\pm 0.018\pm 0.007$
	1.94	1.23	30 ± 19	1	$0.030\pm 0.019\pm 0.007$
	2.31	1.20	26 ± 22	11	$0.031\pm 0.026\pm 0.005$
	2.69	1.18	28 ± 22	0	$0.038\pm 0.030\pm 0.004$
	3.06	1.15	72 ± 22	0	$0.112\pm 0.034\pm 0.013$
	3.44	1.12	19 ± 22	3	$0.034\pm 0.038\pm 0.004$
	3.81	1.09	27 ± 21	2	$0.053\pm 0.041\pm 0.006$
	4.19	1.07	42 ± 21	2	$0.089\pm 0.044\pm 0.010$
	4.56	1.04	34 ± 21	1	$0.080\pm 0.048\pm 0.008$
4.94	1.01	50 ± 20	1	$0.126\pm 0.051\pm 0.015$	

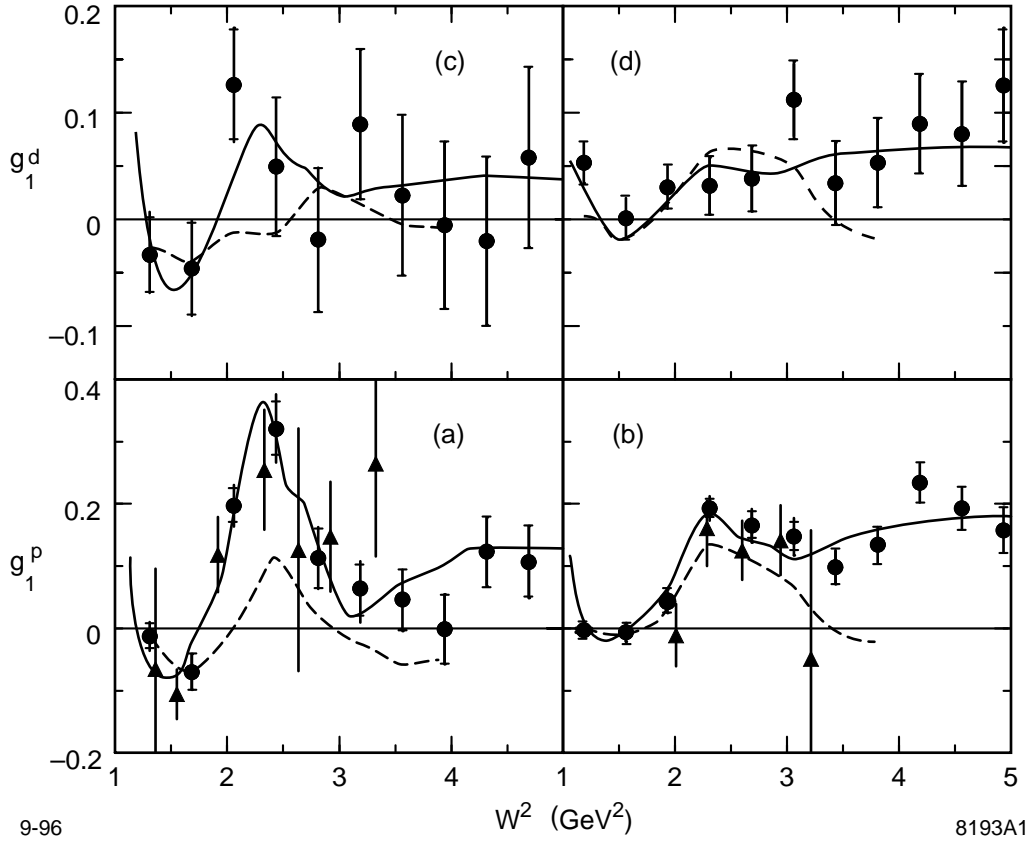
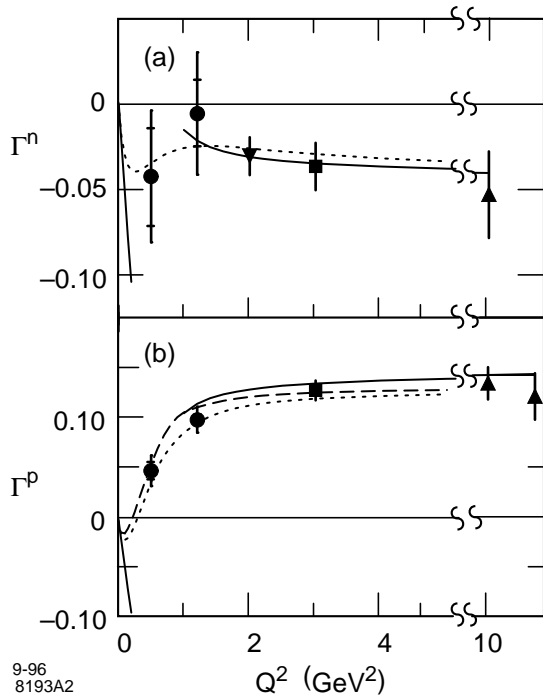


Fig. 1. Measurements of g_1 as a function of W^2 for the proton at (a) 4.5° and (b) 7° ; and for the deuteron at (c) 4.5° and (d) 7° . The present data (circles) are plotted together with the data of Baum *et al.* (triangles), our Monte Carlo simulation (solid line), and the model AO of Burkert and Li [15] (dashed line). The full error bars correspond to statistical and systematic errors added in quadrature, whereas the cross bars indicate statistical errors only.



9-96
8193A2

Fig. 2. Integrals of g_1 at several fixed values of Q^2 for (a) the neutron and (b) the proton. The present data (circles) are plotted together with data from CERN [4] (triangles), E143 deep-inelastic [5] (squares), and E142 [3] (inverted triangle). The curves correspond to the evolution [21] of the deep-inelastic results due to changing α_s (solid line), the predictions of Burkert and Ioffe [19] (dotted line), the model of Soffer [20] (dashed line), and the GDH approach to $Q^2 = 0$ (solid line). Errors are indicated as in Fig. 1.